Magnetic structure of $Fe_{1-x}Co_xSi$ in a magnetic field studied via small-angle polarized neutron diffraction

S. V. Grigoriev,[1] V. A. Dyadkin,[1] D. Menzel,[2] J. Schoenes,[2] Yu. O. Chetverikov,[1] A. I. Okorokov,[1] H. Eckerlebe,[3] and S. V. Maleyev[1]

[1]*Petersburg Nuclear Physics Institute, Gatchina, 188300 St-Petersburg, Russia*

[2]*Institut für Physik der Kondensierten Materie, Technische Universität Braunschweig, D-38106 Braunschweig, Germany*

[3]*GKSS Forschungszentrum, 21502 Geesthacht, Germany*

(Received 24 May 2007; revised manuscript received 21 July 2007; published 21 December 2007)

The magnetic structure of $Fe_{1-x}Co_xSi$ single crystals with $x=0.10, 0.15, 0.20, 0.50$ has been studied by small angle polarized neutron diffraction and superconducting quantum interference device measurements. Experiments have shown that in zero field the compounds with $x=0.1, 0.15$ have a well-defined tendency to order in the one-handed spiral along $\langle 100 \rangle$ axes due to the anisotropic exchange, that, however, decreases with increasing Co concentration x. The magnetic structure of $Fe_{1-x}Co_xSi$ with $x=0.2, 0.5$ consists of spiral domains with randomly oriented spiral wave vector **k**. The applied magnetic field produces a single domain helix oriented along the field. The process of the reorientation starts at the field H_{C1}. Further increase of the field leads to a magnetic phase transition from a conical to a ferromagnetic state near H_{C2}. In the critical range near T_C the integral intensity of the Bragg reflection shows a well-pronounced minimum at H_{fl} attributed to a **k** flop of the helix wave vector. On the basis of our experiments we built the H-T phase diagram for each compound. It is shown that the same set of the parameters governs the magnetic properties of these compounds k, H_{C1}, H_{fl}, and H_{C2}. Our experimental findings are well interpreted in the framework of a recently developed theory [Phys. Rev. B **73**, 174402 (2006)] for cubic magnets with Dzyaloshinskii-Moriya (DM) interaction. In particular, the theory suggests an additional quantum term in the magnetic susceptibility caused by the DM interaction which is in good agreement with the experiment.

DOI: 10.1103/PhysRevB.76.224424 PACS number(s): 75.40.−s, 61.12.Ex

I. INTRODUCTION

One of the most interesting problems in condensed matter physics for the past decade is the paradigm of quantum phase transitions (QPT). In particular MnSi, the cubic magnet with Dzyaloshinskii-Moriya (DM) interaction, has attracted much of the researchers' attention. This system MnSi is known to suffer the QPT under the hydrostatic pressure P as the magnetic order disappears upon increase of P ($T_C \to 0$ at $P \to P_c \approx 15$ kbar).[1,2] In spite of the great interest neither the role playing by the DM instability in this QPT was clarified nor any other parameter, which is responsible for the QPT, has been established. Similar to the pressure effect in MnSi, the variation of the cobalt concentration x in the compound $Fe_{1-x}Co_xSi$ results in a strong change of T_C. The magnetic structure of these compounds are well explained in the Bak-Jensen model that takes into account the hierarchy of the interactions:[3] The exchange interaction, the isotropic Dzyaloshinskii-Moriya (DM) interaction and the weak anisotropic exchange (AE) interaction. Therefore, studying the magnetic properties of $Fe_{1-x}Co_xSi$, which are related to these principal interactions, and following their interplay and their relation to T_C would shed a new light on the QPT both in MnSi and relative systems.

The cubic B20-type mixed compound $Fe_{1-x}Co_xSi$ with $x > 0.05$ orders below T_C in a one-handed spin helical structure with a small propagation vector $k < 0.025$ Å^{-1} (Refs. 4–7) (see Fig. 1). At present it is widely recognized that in analogy to the magnetic structure of MnSi (Ref. 8 and 9) and FeGe,[10] the helicity is induced by an antisymmetric Dzyaloshinskii-Moriya (DM) exchange interaction caused by the lack of a center of symmetry in the arrangement of magnetic atoms Fe and Co.[3,11,12] This DM interaction is isotropic in cubic crystals and a weak anisotropic exchange (AE) interaction along with cubic anisotropy should fix the direction of the magnetic spiral below T_C.[3] However, the AE interaction and cubic anisotropy are extremely weak in this compound and the spiral wave vector **k** is almost randomly oriented. Its direction can be changed by an applied magnetic field. On the other hand, recent investigations of the magnetic structure of $Fe_{0.5}Co_{0.5}Si$ by Lorentz electron microscopy allowed to visualize the helical spin order in real space and had shown a tendency of the propagation vector **k** to orient along [100] axis when the sample is frozen in a small magnetic field of an arbitrary direction ($H < 0.1$ mT).[13]

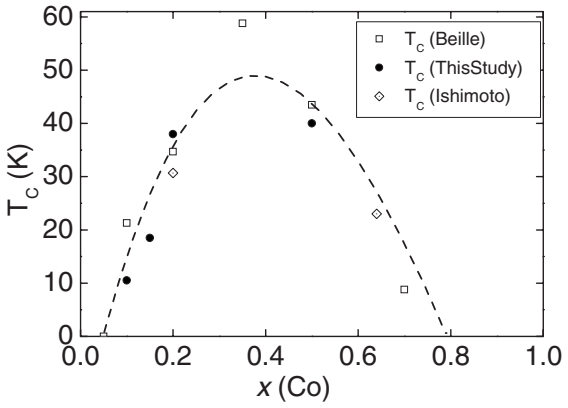

FIG. 1. Critical temperature T_C as a function of the Co concentration x [□ (Refs. 4 and 5); △ (Refs. 6 and 7); • is this study].

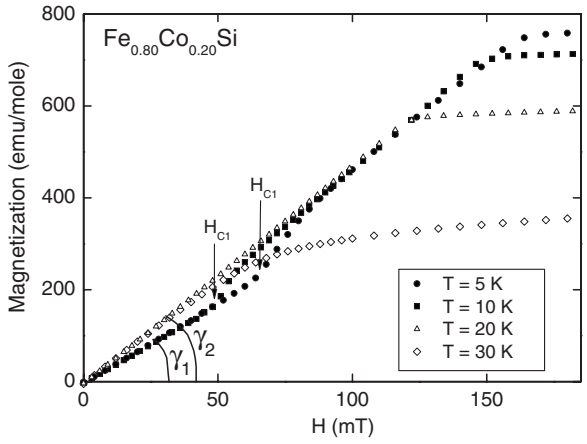

FIG. 2. Field dependent magnetization curves taken at different temperatures T=5, 10, 20, 30 K for $Fe_{0.8}Co_{0.2}Si$.

The magnetic properties of $Fe_{1-x}Co_xSi$ under applied magnetic field were studied in detail, particularly for x=0.2.[6,7] The H-T phase diagram, being built as a result of the measurements, showed much similarity to that of MnSi.[8] As was shown in Refs. 6 and 7 for x=0.2, the magnetic helical structure becomes a single-domain conical structure in a magnetic field $H_{C1} \simeq 60$ mT at low temperature. The cone angle decreases as the field increases and an induced ferromagnetic state appears at $H_{C2} \simeq 170$ mT. The period of the helix does not change with the field. In addition, a **k** flop of the helix wave vector was found in the field range $H_{\mathrm{fl}} \sim 30-50$ mT slightly below T_C in full analogy to that in MnSi.[14–16] This **k** flop reveals itself as a 90° reorientation of the spiral wave vector **k** from the direction parallel to the field to the direction perpendicular to it in both case of $Fe_{0.8}Co_{0.2}Si$ (Ref. 6) and MnSi.[16] This phenomenon had been named as the appearance of an A phase and was wrongly interpreted as having a paramagnetic nature (see Ref. 16 for details).

Although these compounds have been extensively studied, up to now their properties remain puzzling due to the lack of a microscopic quantitative description of the obtained experimental results. In particular, from one hand, a crossover behavior of the magnetic susceptibility near $H \leqslant H_{C1}$ has been observed but not interpreted yet (see Fig. 2). On the other hand, the nature of the A phase observed at T_C was not clarified until recently, when the theory of the cubic magnet without center of symmetry was developed[17] and the interaction of the spin helix with the magnetic field was thoroughly considered. In this theory the ground state energy and the spin wave spectrum were evaluated showing, that (i), in accord with Ref. 3, the system is stabilized in the helical ordering due to conventional exchange and DM interaction with the helix wave vector $k=SD/A$ where D is the strength of DM interaction and A is the spin-wave stiffness at momenta $q \gg k$. (ii) The energy landscape of the weak anisotropic interactions, coming from the cubic symmetry, plays a key role in the orientation of the helix wave vector **k**. (iii) The systems with the DM interaction are unstable with respect to the small magnetic field applied perpendicular to **k** unless it is stabilized via a small spin wave gap in the spin wave spectrum.

This paper is aimed to study the magnetic structure of $Fe_{1-x}Co_xSi$ single crystals of different concentrations x =0.10, 0.15, 0.20, 0.50. Using the data of small angle polarized neutron diffraction and SQUID measurements we built the H-T phase diagram for these compounds. We show that the same set of the parameters (k, H_{C1}, H_{fl}, and H_{C2}) characterizes the magnetic properties of these compounds. We show also that both phenomena of the crossover of the susceptibility at low T and the appearance of the A phase at high $T \sim T_C$ have the same origin. Both of them are consequences of un unusual form of the magnetic energy of the helical structure, which is given per unit cell by the expression[17]

$$E_{mag} = -g\mu_B S\left[\frac{H_{\parallel}^2}{2H_{C2}} + \frac{H_{\perp}^2\Delta^2}{4H_{C2}[\Delta^2 - (g\mu_B H_{\perp})^2/2]}\right] + GL(\hat{k}), \tag{1}$$

where S is the total spin of the unit cell, $H_{\parallel}$ and $H_{\perp}$ are the field components along and perpendicular to the helix wave vector **k**, Δ is the spin wave gap, $L(\hat{k}) = 2\sin^2\vartheta(\sin^2\varphi\cos^2\varphi + \cos^2\vartheta)$ is a cubic invariant determining the **k** orientation relative to the crystal axes (ϑ and φ are the corresponding angles) and G is the strength of the anisotropic interactions determined by the cubic anisotropy and the anisotropic exchange (see Ref. 17). The first term with $H_{\parallel}$ is a classical part of the Zeeman energy. The second one has a quantum origin and it describes the interaction of the field, perpendicular to **k**, with the helix as an individual entity. The second term in Eq. (1) implies the presence of a small spin wave gap Δ and explains the existing puzzles. In our present study we check the applicability of the theory,[17] which allows an indirect determination of the spin wave gap predicted to exist in compounds with DM interaction.

It is worthwhile to note that the recent study of a single atomic layer of manganese on tungsten demonstrated the existence of the spin spiral structure with the long period of 12 nm instead of antiferromagnetic ordering, which is characteristic for Mn. This observation was interpreted through appearance of the DM interaction on magnetic surfaces because such surface lacks obviously the inversion symmetry.[18] This finding changes the whole concept of the magnetic structures in nanomagnetism as it introduces an important DM interaction into the consideration of nanoobject's properties. The theoretical approach, which is applied to explain this phenomenon, is similar to that made by Bak and Jensen[3] for the interpretation of the spiral structure in MnSi. Therefore, new theoretical and experimental efforts to describe and to understand the fascinating behavior of MnSi-type compounds are of great interest as they become the model systems for magnetic low-dimensional and nanoscale objects.

The paper is organized in the following way. Section II describes the preparation of the samples, the experimental setup, the geometry of the experiment and the qualitative picture of the polarized SANS measurements. The analysis of the data obtained are performed and shown in Sec. III. This analysis leads to the H-T phase diagram, which is discussed in Sec. IV on the basis of the theory.[17] Section VI contains the summary and the conclusion.

II. EXPERIMENT

A. Samples

A series of $Fe_{1-x}Co_xSi$ single crystals with $x=0.10, 0.15, 0.20, 0.50$ (at. %) were chosen for the study. They were cut from large single crystals, which were grown by the tri-arc Czochralski method. The critical temperature T_C has been obtained from the neutron scattering measurements as the temperature, where the magnetic Bragg reflection disappears. The values of T_C for different concentrations x are plotted in Fig. 1 along with those given in the other studies.[4–7] It is well known that up to a Co concentration of approximately 5 at. % $Fe_{1-x}Co_xSi$ is a paramagnetic semiconductor, while above 5 at. % this compound becomes magnetically ordered and a metallic system.[19,20] Thus the magnetic and transport properties of these compounds are strongly correlated showing also a positive magnetoresistive effect in the ordered phase.[21] The critical temperature T_C increases rapidly upon doping with Co, has its maximum value near 60 K at $x=0.35$ and then decreases smoothly and diminishes to $T=0$ at $x=0.8$. There is a certain disagreement between the values given by different authors for the equal concentration x. This disagreement may be explained taking into account that the samples could be of different purity and that Co atoms dissolve inhomogeneously in the solid solution.

All samples were magnetically characterized by SQUID magnetometry. Figure 2 shows magnetization curves taken at different temperatures below $T_C=38$ K for the sample with $x=0.2$. For the low temperature measurements at $T=5$ K and 10 K the linear behavior of the magnetization with the slope γ_1 in the range of small field vanishes above H_{C1} and transforms into the linear dependence with the slope γ_2. This type of behavior is not observed for the high-temperature curves at $T=20$ and 30 K with a constant slope equal to γ_2 both for small and large fields. The curves saturate at the critical field H_{C2} indicating the field-induced phase transition from the conical to the ferromagnetic state. Upon decreasing the field, no break of the magnetization curve is observed and the magnetization decreases linearly with the slope γ_2 to its zero field value demonstrating a hysteresis in the field range $H \sim H_{C1}$ (not shown in Fig. 2). This behavior of the magnetization is typical for all samples and was also observed in the previous studies.[4–7] The explanation of this phenomenon will be given below on the basis of the theory[17] and neutron diffraction data.

B. Polarized SANS: Technique

The polarized SANS experiments were carried out at the SANS-2 scattering facility of the FRG-1 research reactor in Geesthacht (Germany). A polarized beam of neutrons with an initial polarization $P_0=0.95$, a neutron wavelength $\lambda=0.58$ nm, a bandwidth $\Delta\lambda/\lambda=0.1$, and a divergence $\eta=2$ mrad was used, leading to a transverse resolution of 0.1° in a rocking scan. The scattered neutrons were detected by a position sensitive detector with 256×256 pixels. The detector-sample distance was set such that the q range was covered from 1×10^{-3} to 1 nm^{-1} with a step of 0.001 nm^{-1}. The scattering intensity was measured in the temperature range $8\ \mathrm{K} < T \leqslant 60$ K with an accuracy better than 0.05 K.

The neutron elastic cross section per unit cell of the magnetic helix below T_C has the following form:[22]

$$\frac{d\sigma}{d\Omega} = \left(\frac{rS}{2}\right)^2 \frac{(2\pi)^3}{V_0}\{[1+(\hat{q}\hat{c})^2 - 2(\hat{q}\mathbf{P}_0)(\hat{q}\hat{c})]\delta(\mathbf{q}-\mathbf{k}) + [\mathbf{P}_0 \rightarrow -\mathbf{P}_0]\delta(\mathbf{q}+\mathbf{k})\}\sin^2\alpha, \quad (2)$$

where $r=0.54\times10^{-12}$ cm, S and $V_0=a^3$ are the spin and volume of the unit cell, respectively, $\hat{q}=\mathbf{q}/|q|$ is the unit vector of the momentum transfer, $\hat{c}$ is the unit vector of the helix axis $\mathbf{k}$, $\mathbf{P}_0$ is the vector of polarization, $\alpha=\pi/2-\beta$ is determined through the cone angle β, and $\delta(\mathbf{q}\mp\mathbf{k})$ enforces the Bragg conditions.

For the single-handed helical structure the neutron cross section depends on the incident polarization $\mathbf{P}_0$. For example, if $\mathbf{P}_0$ is along $\hat{c}$ and $P_0=1$, the scattering is forbidden for $\mathbf{q}=\mathbf{k}$ but is maximal for $\mathbf{q}=-\mathbf{k}$. When $\mathbf{P}_0\perp\hat{\mathbf{c}}$, the scattering does not depend on the polarization. In intermediate cases the polarization of the neutron scattering is determined as

$$P = \frac{\sigma(\mathbf{P}_0)-\sigma(-\mathbf{P}_0)}{\sigma(\mathbf{P}_0)+\sigma(-\mathbf{P}_0)} = (\hat{q}\mathbf{P}_0) = \cos\phi, \quad (3)$$

where ϕ is the angle between the incident polarization and the scattering vector. This equation is valid for all measurements presented below for $T<T_C$.

We have investigated experimentally the intensities with the polarization along $[I(q,P_0)]$ and opposite $[I(q,-P_0)]$ to the magnetic field. The measured scattering is characterized by two quantities: (i) The intensity of the scattering: $I=[I(P_0)+I(-P_0)]$ and (ii) the polarization of the scattering: $P=[I(P_0)-I(-P_0)]/[I(P_0)+I(-P_0)]$.

In absence of the field the magnetic structure of $Fe_{1-x}Co_xSi$ consists of spiral domains, which are either randomly oriented for some concentrations[4–7] or have a slight preference to orient along the cube edges: $\mathbf{k}\|\langle100\rangle$[13]. In our experiment, the samples (single crystals) were oriented in such a way that at least one axis $\langle100\rangle$ was set in a plane perpendicular to the incident beam (Fig. 3). In the case of scattering from magnetic spirals with a long period, this geometry allows one to observe diffraction peaks in a range of small-angle scattering, provided that the Bragg condition is fulfilled: $2d\sin(\theta_B/2)=\lambda$, or $q=2\pi/d$, where d is the period of the spiral and θ_B is the scattering angle. The external magnetic field H from 1 to 200 mT was applied horizontally and perpendicular to the incident beam and the neutron polarization followed the direction of the magnetic field.

C. Polarized SANS: Measurements

Figure 4 shows maps of SANS intensities for four different $Fe_{1-x}Co_xSi$ samples with (a) $x=0.10$, (b) $x=0.15$, (c) $x=0.20$, and (d) $x=0.50$ at $T\approx9$ K. A weak magnetic field of $H\simeq1$ mT was applied horizontally in the plane of the detector. It is clearly seen from Fig. 4(a) that in $Fe_{0.90}Co_{0.10}Si$ the spiral wave vector $\mathbf{k}$ is oriented along the axis [1 0 0], which is inclined 25° to the field direction. In $Fe_{0.85}Co_{0.15}Si$ [Fig. 4(b)] the spiral wave vector $\mathbf{k}$ is oriented along the [1 0 0]

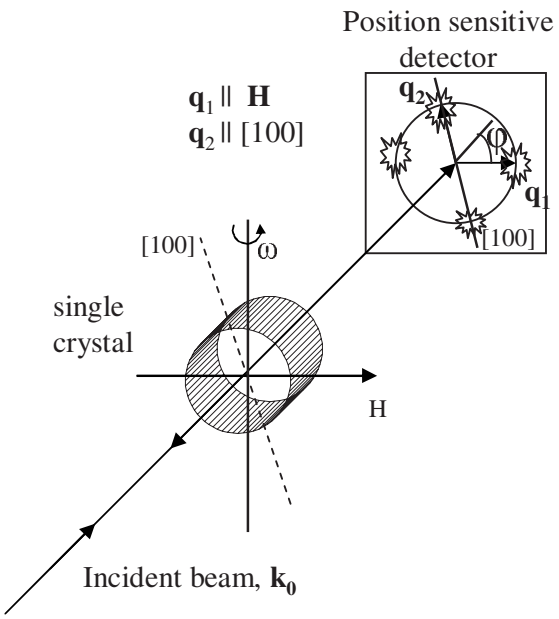

FIG. 3. Schematic outline of the experiment: the $Fe_{1-x}Co_xSi$ single crystals were oriented such that at least one of the axes ⟨100⟩ was perpendicular to the incident beam. The magnetic field **H** was applied horizontally and also perpendicular to the incident beam. The polarization **P** followed the direction of the magnetic field.

and [0 1 0] axes, which are inclined at 35° and 55° to the field direction, respectively. The Bragg peaks are, however, strongly smeared, having a clear tendency to form a ring of a radius $|\mathbf{k}|$. In $Fe_{0.80}Co_{0.20}Si$ [Fig. 4(c)] the spiral wave vector **k** is almost randomly oriented and the scattering looks like a ring of the intensity. In $Fe_{0.50}Co_{0.50}Si$ [Fig. 4(d)] the spiral wave vector **k** is oriented along the weak field of 1 mT and

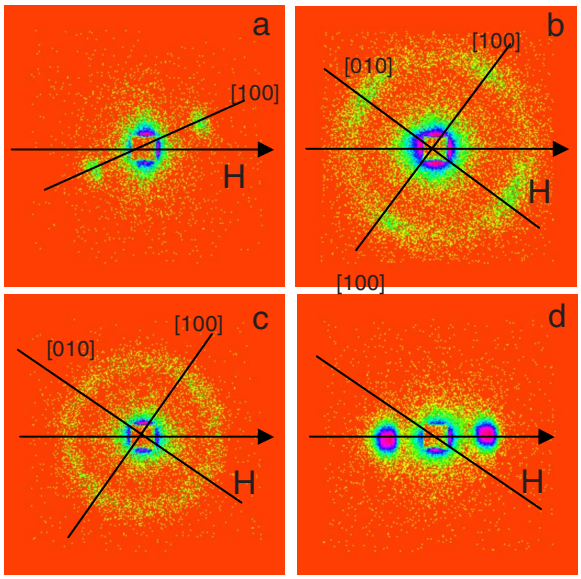

FIG. 4. (Color online) Maps of the SANS intensities for $T \approx 9$K for four different samples $Fe_{1-x}Co_xSi$ and (a) $x=0.10$, (b) $x=0.15$, (c) $x=0.20$, and (d) $x=0.50$. A weak magnetic field of $H \sim 1$ mT is oriented horizontally in the plane of the detector.

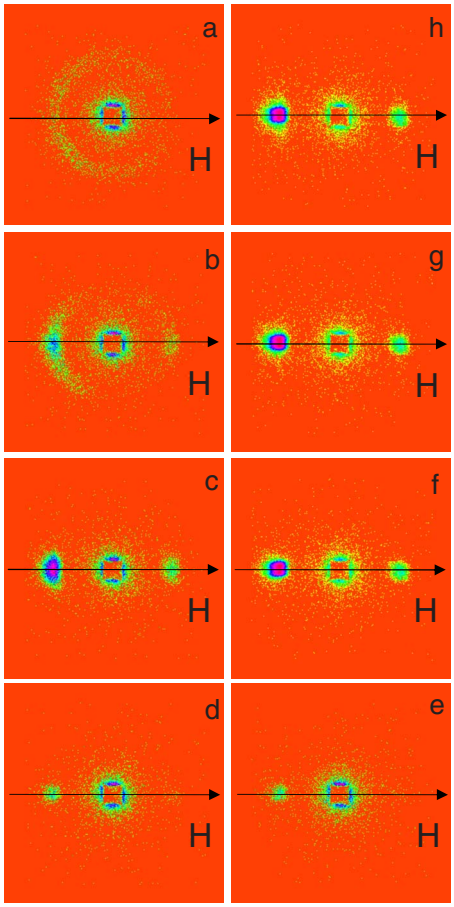

FIG. 5. (Color online) Maps of the SANS intensities for $x=0.2$ at $T=10$ K for eight values of magnetic field: (a), (h) $H=0$ mT; (b), (g) $H=50$ mT; (c), (f) $H=100$ mT; (d), (e) $H=170$ mT. The magnetic field increases from (a) to (d) and decreases from (e) to (h).

the scattering intensity is concentrated into two Bragg spots with $\mathbf{k} \parallel \mathbf{H}$. Thus a clear tendency in the spiral orientation is observed with increase of Co concentration. The anisotropic exchange and crystallographic anisotropy play a dominating role in the orientation of the spiral wave vector **k** for compounds with small concentrations of Co. For concentrations of $x \sim 0.1$ the substitution of Co does not break the preferable anisotropy axes ⟨100⟩. The increase of the substituted atoms up to $x \sim 0.2$ results in a local disorder and therefore in the random orientation of **k**. Further increase of the Co concentration results in full suppression of the anisotropy so that a weak magnetic field of 1 mT prevails over the anisotropy energy and orients **k** along the field for $x=0.5$. Thus one concludes that the anisotropy is suppressed with an increase of the Co concentration.

The typical magnetic field behavior of the spiral structure of these compounds is shown in Fig. 5. As an example, the sample with $x=0.2$ at $T=10$ K has been chosen. When a weak magnetic field $H \leqslant 60$ mT is applied, the randomly oriented spirals remain frozen in spite of the applied field, and scattering intensity is formed as a ring on the map [Fig. 5(a)]. When the field **H** increases above $H_{C1}=60$ mT the randomly oriented domain structure transform into a single domain

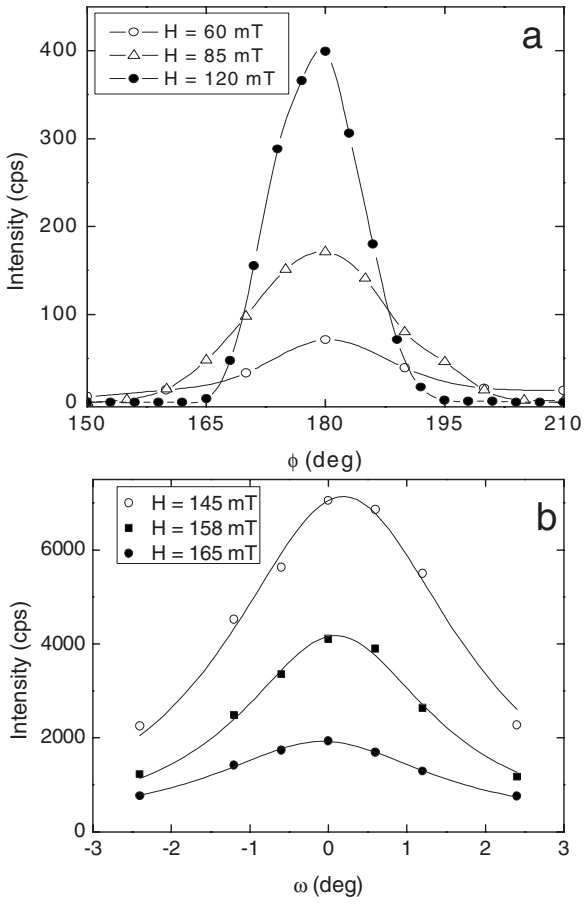

FIG. 6. (a) Neutron intensitiy along the ring at $q=|q_c|$, i.e., as a function of the angle between **H** and **q** for $Fe_{0.8}Co_{0.2}Si$ at $T=10$ K and $H=60$, 85, and 120 mT. Lines corresponds to Gaussian functions. (b) Rocking curves of the magnetic Bragg reflections $I(\omega)$ (ω is a rocking angle) ($\mathbf{k}\|\mathbf{H}$) at $T=10$ K for $H=145$, 158, and 165 mT upon increase of the magnetic field. The lines correspond to the Lorentzian functions.

sample. The ring of the intensity transforms smoothly into spots laying on the field axis [Figs. 5(b) and 5(c)]. With further increase of the field above $H_{C2}=175$ mT the reflections along the field vanishes that is the helix transforms into an induced ferromagnet.

Upon decrease of the field H to zero the sample remains a single domain showing a large hysteresis in the scattering intensity [Figs. 5(e)–5(h)]. In particular, no ring appears but the Bragg spots remain and their intensity increases upon decrease of the magnetic field. The details of the reorientation process are presented below in the data analysis of the temperature and magnetic field scans.

III. DATA ANALYSIS

To illustrate a typical behavior of the neutron scattering patterns we plot the intensity along the ring at $|\mathbf{q}|=k$ (shown in Fig. 5) as a function of the angle ϕ for different values of the magnetic field and at $T=10$ K [Fig. 6(a)]. Here ϕ is an angle between the magnetic field axis and the scattering vector **q**. The scattering has a maximum in the directions of the

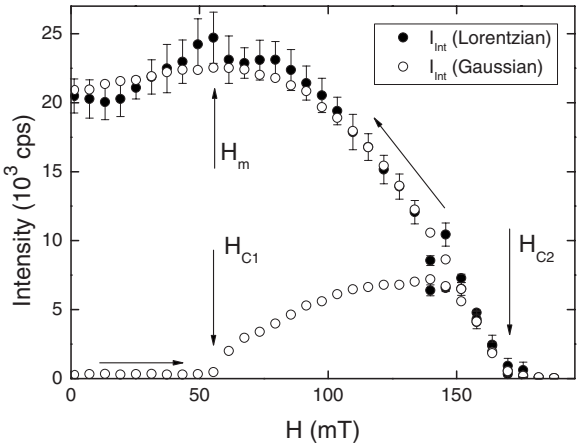

FIG. 7. Integral intensity of the Bragg peak ($\mathbf{k}\|\mathbf{H}$) at $T=10$ K for $Fe_{0.8}Co_{0.2}Si$ upon increase and subsequent decrease of the magnetic field H.

field at $H<H_{C1}$, and the intensity is well fitted by the Gaussian:

$$I(\phi) = I_{\mathrm{BG}} + \sqrt{\frac{2}{\pi}}\frac{I_{\mathrm{int}}}{\delta_M}\exp\left(-2\frac{(\phi-\phi_c)^2}{\delta_M^2}\right), \qquad (4)$$

where I_{BG} is a background intensity. The integral intensity I_{int}, the center of Gaussian ϕ_c, and the full width at half maximum (FWHM), or mosaic of the helix structure δ_M, were obtained from the fit. It is also important to note that the scattering is fully polarized at $\phi=0°$ ($P\rightarrow+P_0$) and at $\phi=180°$ ($P\rightarrow-P_0$).

The integral intensity I_{int} is plotted in Fig. 7 (open symbols) as a function of the field. At zero field the intensity is very low, since the scattering is almost homogeneously distributed over the sphere with radius $q=k$. No change in the scattering intensity is observed at $H<H_{C1}=60$ mT, so the field increase is not able to change the frozen helix domain structure with the random distribution of the **k** orientation. The intensity goes up slowly upon increase of the field in the range from 60 to 140 mT, showing the process of the reconstruction from the multidomain to the single domain structure. Then the intensity of the scattering decreases to zero at the second critical field $H_{C2}=175$ mT, where the sample transforms into the ferromagnetic state. The change of the mosaic δ_M and the position of the Bragg reflection ϕ_c upon increase of the magnetic field is shown in Fig. 8. Both δ_M and ϕ_c are ill-defined quantities at $H<H_{C1}$. Further on, the mosaic δ_M decays strongly from the value of 40° at $H=H_{C1}$ to the resolution limit of the order of 10° at $H=140$ mT. The center of the Gaussian ϕ_c remains constant in the whole range from $H=H_{C1}$ up to $H=H_{C2}$. The backward decrease of the magnetic field leads to the significant hysteresis in the integral intensity I_{int} (Fig. 7). The intensity increases in the field range from H_{C2} to H_m (the field of the maximum) and then decreases slightly upon reduction of the field to zero. Neither the position of the Gauss peak nor its width (FWHM) change with the decrease of the magnetic field. Thus these measurements remain resolution limited. It

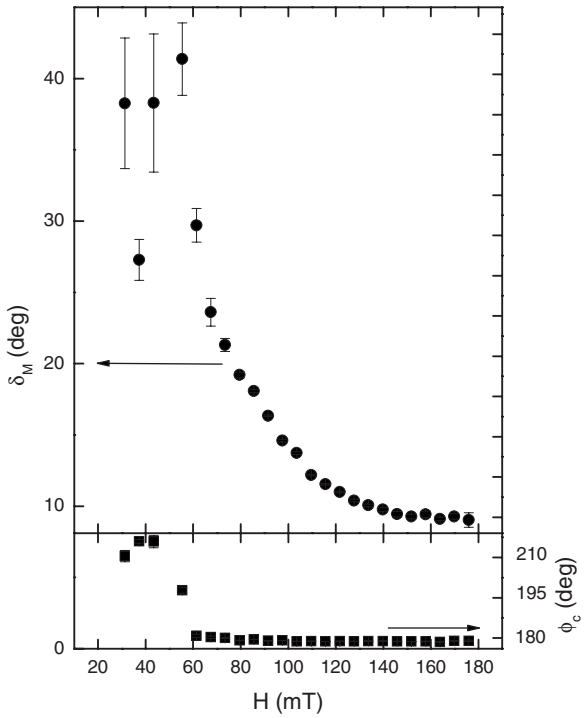

FIG. 8. Center of the Gaussian peak ϕ_c (a) and the magnetic mosaic δ_M (b) of the magnetic Bragg reflection ($\mathbf{k}\|\mathbf{H}$) as a function of the magnetic field. The data are not corrected for resolution.

should also be noted that the value of the helix wave number k does not change with the magnetic field and that the polarization is constant in the whole range $H<H_{C2}$.

The resolution limit (FWHM of 10°) in measurements of the orientation spread δ_M of the wave vector $\mathbf{k}$ is not the "true" instrumental limit of the setup but is a treatment-dependent level of the resolution. The scale, which is used in this treatment, runs from 0 to 360° with steps of about 5° determined by the size of the direct-beam spot and the radius of the scattering ring. Indeed, the real resolution limit of the setup is 0.1°. Therefore, one can improve significantly the accuracy of the measurements if one performs a rocking scan experiment. In such an experiment one should take into account that the magnetic structure of the $Fe_{1-x}Co_xSi$ system under applied field has a complicated and irreversible behavior. Therefore, it is important that the magnetic history of the sample is always uniquely defined. We performed the measurements in the following way: (i) Zero field cooling (ZFC) from the paramagnetic state to the temperature of interest T; (ii) rising up the field from $H=0$ to the field of interest; and (iii) the field direction is fixed with respect to the sample in the rocking scan experiment.

The rocking curves of the Bragg peak oriented along the field were taken in the range (±3° with the step of 0.5° and an accuracy of 0.1°) at different values of the field at $T=10$ K. It is clear from Figs. 6 and 8 that the mosaic of the helix structure is much larger than the range run in the rocking scan experiment for the field increasing from 0 to 140 mT. Therefore the rocking scan measurement in this field range is senseless and shows a "plateau" of intensity within the range of measured angles ±3°. A well-defined maximum in the range of rocking curve experiment appears in the upward regime of measurements at $H\geqslant 140$ mT and in the downward regime in the whole field range. The curves for the upward regime are plotted in Fig. 6(b) and well fitted by the Lorentz function:

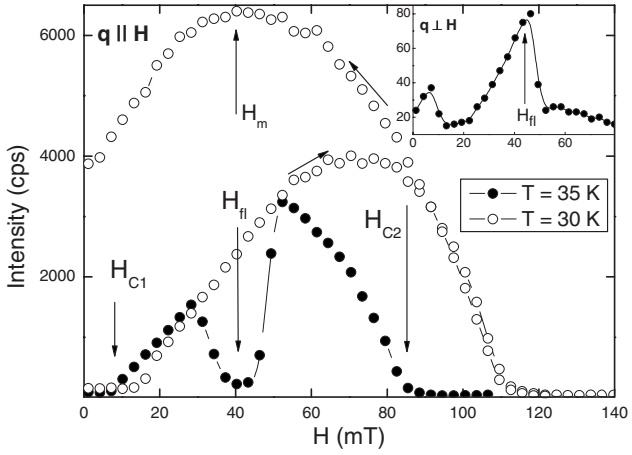

FIG. 9. Integral intensity of the Bragg peak ($\mathbf{k}\|\mathbf{H}$) at $T=30$ and 35 K for $Fe_{0.8}Co_{0.2}Si$ as a function of the magnetic field H. At $T=30$ K the intensity shows a maximum at $H_m=40$ mT upon decrease of the field. The inset shows the intensity of the Bragg peak at $\mathbf{k}\perp\mathbf{H}$.

$$I(\omega) = I_{\mathrm{BG}} + \frac{2I_{\mathrm{int}}}{\pi}\frac{\delta_M}{4(\omega-\omega_c)^2+\delta_M^2}, \tag{5}$$

where I_{BG} is a background intensity, ω is a rocking angle, ω_c is a center of peak, and δ_M is a FWHM. The integral intensity I_{int} obtained from the fit is plotted in Fig. 7 (closed symbols). The intensity obtained in the rocking scan coincides practically with that taken from the Gaussian function. Thus, the rocking scan experiment shows the Lorentzian distribution of the neutron scattering intensity around the field axis in the single domain state. The width of the Lorentzian peak does not depend on the magnetic field but the Lorentzian shape implies smeared or smooth boundaries between different coherent volumes.

Thus we follow the transformation from randomly oriented helix domains toward a single domain structure. In zero field (after ZF cooling) a ring of the intensity in the neutron scattering experiment occurs representing a system of randomly oriented helix domains. It is shown that the process of the magnetization is characterized by several features at H_{C1} (the threshold field for the domain reorientation), H_{C2} (the critical field of the transition to the ferromagnetic state), and H_m (the field of maximal intensity). The field dependence of the neutron scattering intensity was measured at different temperatures below T_C. The behavior similar to that described for the field dependence at $T=10$ K was observed for all magnetic field scans except that at $T=35$ K, i.e., close to $T_C=38$ K. Figure 9 shows the field dependence of the integral intensity of the Bragg peak ($\mathbf{k}\|\mathbf{H}$) at $T=30$ and 35 K. In the scan at $T=35$ K the integral intensity I_{int} has

a well-pronounced minimum at $H_{fl} \simeq 40$ mT. In the same field range near H_{fl} two weak spots appear in the direction perpendicular to the field (see the inset in Fig. 9). The length of the helix wave vector for these two spots ($\mathbf{k} \perp \mathbf{H}$) is the same as for the major reflections with ($\mathbf{k} \| \mathbf{H}$). Since the intensities are much weaker than that of the normal reflection we suppose, in accordance with Ref. 6, that these spots are the cross sections of a ring around the field axis. It is important to note that for $T=30$ K no minimum is observed when the field increases. Nevertheless, the intensity shows a maximum at $H_m=40$ mT upon a decrease of the field. This behavior at $T=30$ K clearly demonstrates that the field $H \simeq 40$ mT is characteristic not only for the critical temperature range but also for the low temperatures. This phenomenon, often called *A* phase, was also observed in the relative compound MnSi.[16] In our opinion, this demonstrates the flop of the helix wave vector (**k** flop) in a narrow region close to H_{fl}, i.e., the orientation of the helix wave vector along the field becomes less favorable than its orientation perpendicular to the field axis. Such behavior was recently explained in the framework of the theory of cubic magnets with DM interaction[17] and will be discussed later in detail.

Similar measurements of the Bragg intensity as function of the magnetic field were performed for the other compounds under study. Figure 10(a) gives the field dependence of the integral intensity of the Bragg peak ($\mathbf{k} \| \mathbf{H}$) for $Fe_{0.5}Co_{0.5}Si$ at $T=37$, 38, and 39 K. The minimum in the field scan of the integral intensity is registered at $H_{fl} \simeq 8$ mT. This minimum is less pronounced upon a decrease of the temperature and vanishes completely at $T=35$ K. The similar phenomenon is shown in Fig. 10(b) for $Fe_{0.85}Co_{0.15}Si$ at $T=16$ and 17 K. For this compound the minimum is observed at $H_{fl} \simeq 30$ mT. Thus it is indicated that the **k** flop near T_C under an applied field is a common feature for all Co concentrations of the $Fe_{1-x}Co_xSi$ system.

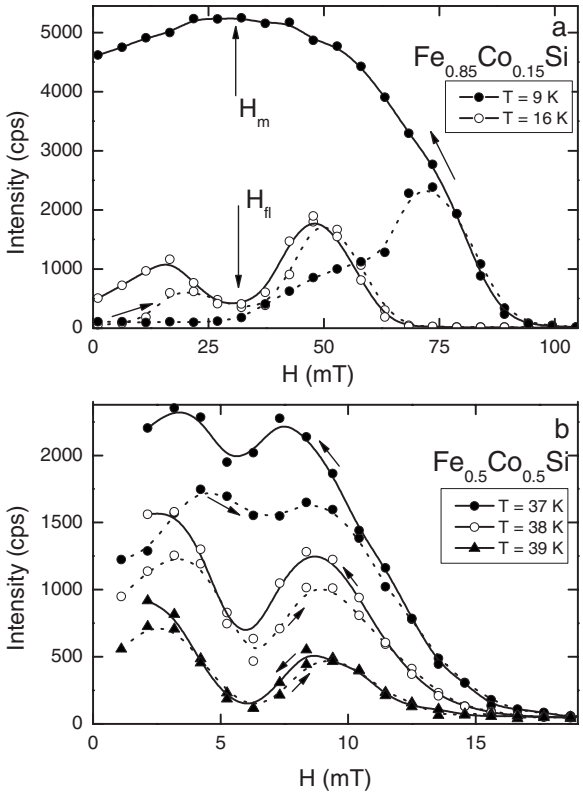

FIG. 10. Field dependence of the integral intensity of the Bragg peak ($\mathbf{k} \| \mathbf{H}$): (a) For $Fe_{0.5}Co_{0.5}Si$ at $T=37$, 38, and 39 K; (b) for $Fe_{0.85}Co_{0.15}Si$ at $T=16$, 17 K. The segment line and the open symbols show the increase of the field, the straight line and the close symbols represent the decrease of the field.

IV. *H-T* PHASE DIAGRAMS

As shown above, the magnetic field changes the spin structure significantly. From the diffraction experiment one can extract the following characteristic fields H_{C1}, H_{C2}, H_{fl}, and H_m. From these data we built the magnetic phase diagram for different compounds $Fe_{1-x}Co_xSi$ with $x=0.5$, $x=0.2$, and $x=0.15$ [Figs. 11(a)–11(c), respectively]. As is well seen from Fig. 11 the similarity of the diagrams for the different compounds are straightforward, i.e., the same set of the parameters characterizes their magnetic properties. It should be noticed that the field H_{C1} was not registered for the compound with $x=0.5$ since it is smaller than 1 mT [Fig. 11(a)].

The most detailed phase diagram was obtained for the compound with $x=0.2$ [Fig. 11(b)]. Above $T_C=38$ K the system is in the paramagnetic phase. After zero field cooling the spiral spin structure with the random orientation of the **k** vector occurs below T_C and at $H<H_{C1}$. Upon increase of the magnetic field the wave vectors **k** of different domains tend to rotate toward the field axis in the region between H_{C1} and H_{C2}. Above H_{C2} the sample becomes ferromagnetic. There is a small region in the *H-T* space below T_C at $H \sim H_{fl}$, where the **k**-vector flops from $\mathbf{k} \| \mathbf{H}$ to $\mathbf{k} \perp \mathbf{H}$. This feature observed close to T_C can only be traced in the low T range at the field H_m, which is the borderline between the single domain spiral state for $H>H_m$ and a slightly disordered state for $H<H_m$ upon decrease of the field from the ferromagnetic state. It is of notable interest that the crossover behavior of the magnetic susceptibility near $H \leqslant H_{C1}$ (Fig. 2) is observed at low temperature only when $H_{C1}>H_m \simeq H_{fl}$. We will interpret these facts in the next section.

An additional parameter obtained from the diffraction experiments is the helix wave vector **k**. Figure 12 shows the temperature dependence of k for different compounds with $x=0.15$, 0.20, and 0.50. k decreases with increasing temperature for the compounds with $x=0.15$ and 0.20 whereas it is constant for $x=0.50$. The value of k is well described by the linear temperature dependence

$$k = k(0)[1 - c(T/T_C)], \tag{6}$$

with $k(0)=0.0185 \pm 0.0001$ Å^{-1} and $c=0.024 \pm 0.002$ for $x=0.20$; with $k(0)=0.0192 \pm 0.0001$ Å^{-1} and $c=0.123 \pm 0.005$ for $x=0.15$; and with $k(0)=0.0058 \pm 0.0006$ Å^{-1} and $c=-0.01 \pm 0.01$ for $x=0.50$.

It is worthwhile to note that k shows the opposite temperature dependence for MnSi.[23] In our view the slope of

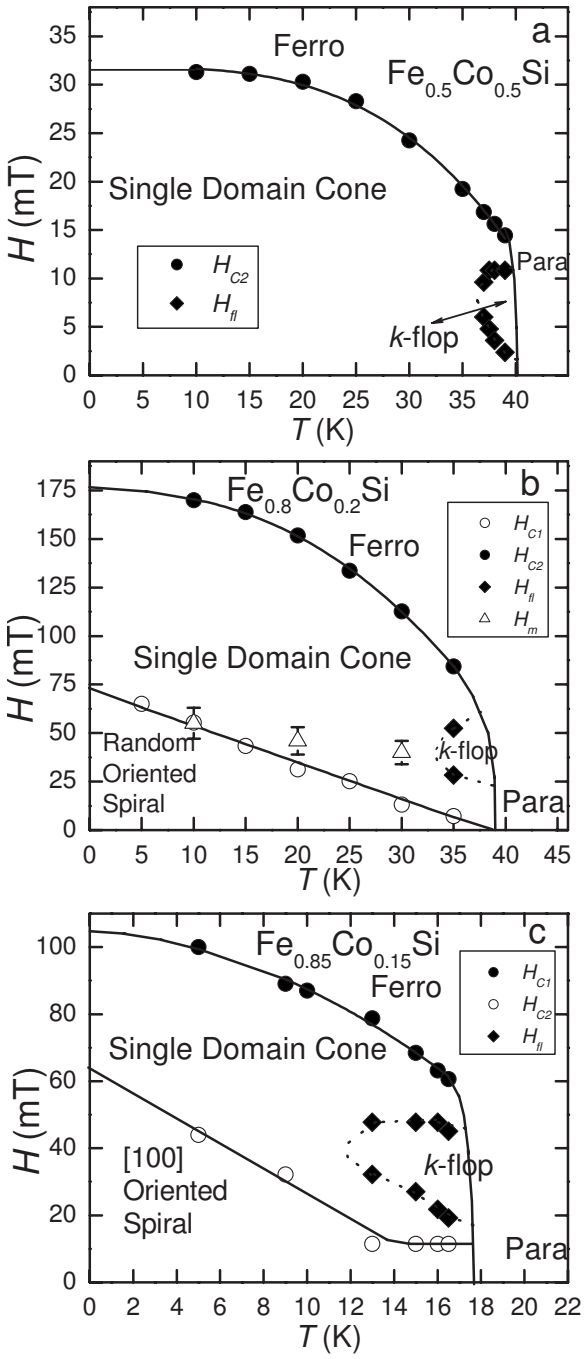

FIG. 11. *H-T* phase diagram for (a) $Fe_{0.5}Co_{0.5}Si$, (b) $Fe_{0.8}Co_{0.2}Si$, and (c) $Fe_{0.85}Co_{0.15}Si$. The compounds are paramagnetic above T_C. Below T_C and at $H<H_{C1}$ a spiral spin structure occurs with the **k** vector either oriented randomly or along the ⟨100⟩ direction. Different domains tend to orient along the field axis in the region between H_{C1} and H_{C2}. Above H_{C2} the sample orders ferromagnetically.

$k(T)$ is related to the sign and the magnitude of the anisotropic exchange F [see Eq. (10) below]. Thus, this anisotropic exchange interaction is a notable value for small x and reduces to zero at large x. This is also confirmed by the observation displayed in Fig. 4.

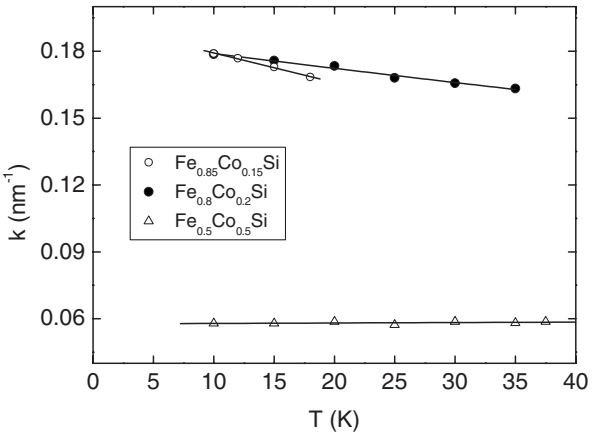

FIG. 12. Temperature dependence of the helix wave vector $|\mathbf{k}|$ at $H=1$ mT for $Fe_{1-x}Co_xSi$ with $x=0.15$, 0.20, and 0.50. The solid line corresponds to the fit as described in the text.

V. INTERPRETATION AND DISCUSSION

A. Principal interactions

As was mentioned in the Introduction these experimental findings are well interpreted within the theory recently developed by one of the authors to describe the properties of cubic helical magnets with DMI in a magnetic field.[17] According to this theory (see also Ref. 16) the magnetic field **H** transforms the spiral into a conical structure with the cone angle $\beta=\pi-\alpha$, where the angle α changes with the field and is determined by

$$\sin\alpha=\begin{cases} H_{\|}/H_{C2}, & \text{if } H_{\|}<H_{C2}, \\ -1, & \text{if } H_{\|}>H_{C2}, \end{cases} \tag{7}$$

where $H_{\|}$ is the field component along the helix axis **k**. For $H_{\|}>H_{C2}$ a ferromagnetic spin configuration occurs. In Ref. 17 it was shown that

$$g\mu_B H_{C2}\approx Ak^2, \tag{8}$$

where A is the spin-wave stiffness at $q\gg k$. At $T=0$ $H_{C2}\simeq 31.3$ mT and $k\approx 0.0058$ Å^{-1} for the compound with $x=0.5$, $H_{C2}\simeq 175$ mT and $k\approx 0.0185$ Å^{-1} for $x=0.2$, and $H_{C2}\simeq 103$ mT, and $k\approx 0.0192$ Å^{-1} for $x=0.15$. Using Eq. (8) one can find that the stiffness $A\approx 110$ meV Å^2 for $x=0.5$, $A\approx 62$ meV Å^2 for $x=0.2$, and $A\approx 34$ meV Å^2 for $x=0.15$.

The value of the helix wave vector is defined as

$$k=S\frac{D}{A}\left(1-\frac{SF}{2A}L(\hat{k})\right)\approx S\frac{D}{A}, \tag{9}$$

where the cubic invariant $L(\hat{k})$ is defined below Eq. (1). Taking the values for A and k, one derives $SD\approx 0.64$ meV Å for $x=0.5$, $SD\approx 1.15$ meV Å for $x=0.2$ and $SD\approx 0.65$ meV Å for $x=0.15$.

Furthermore, one can suggest that the temperature variation of k is connected with the change of the anisotropic constants, which are maximal at $T=0$ and minimal at $T=T_C$. In this case one obtains from Eqs. (6) and (9)

$$c = SFL(\hat{k})/(2A). \tag{10}$$

The k value was measured at very low field where almost a random domain distribution was observed. In this case one has to average L over a random $\mathbf{k}$ orientation and obtains $\bar{L}=3\pi/16$. As a result, $c=3\pi SF/(32A)$ and $SF\approx 0$ meV Å^2 for $x=0.5$, $SF\approx 4.7$ meV Å^2 for $x=0.2$, and $SF\approx 13.4$ meV Å^2 for $x=0.15$. Thus, from the experimental parameters, we are able to determine different contributions to the total energy of the helix structure.

B. k-flop phase

We consider now the evolution of the helical structure in the magnetic field which is expressed by Eq. (1). The term $GL(\hat{k})$, which is responsible for the spin-lattice interaction, plays a dominant role for $H<H_{C1}$, when a local lattice distortion leads to a random orientation of the vector $\mathbf{k}$. At larger fields this term becomes less important. According to Eq. (6) at T close to T_C the field H_{C1} is very small and the L term in Eq. (1) can be neglected. Hence the direction of the helix vector $\mathbf{k}$ is determined by the competition of the first two terms in Eq. (1) which allows one to interpret the $\mathbf{k}$ flop near T_C (A phase).

The analysis of the free energy expression [Eq. (1)] is really straightforward if one rewrites it as

$$E_{\mathrm{mag}} = -\frac{g\mu_B S}{2}\frac{H^2}{H_{C2}}\left[\cos^2\Psi + \frac{\sin^2\Psi}{(2-x^2\sin^2\Psi)}\right],$$

where $x=g\mu_B H/\Delta$ and Ψ is the angle between $\mathbf{k}$ and the magnetic field $\mathbf{H}$. Minimizing this expression with respect to Ψ one can find that at $x<1$ the angle $\Psi=0$. At $x=1$ the magnetic energy has its minima at both $\Psi=0$ and $\Psi=\pi/2$. In the interval $1<x<\sqrt{2}$ the minimum is at $\Psi=\pi/2$. In the range $\sqrt{2}\leqslant x$ the second term in Eq. (1) is unphysical[17] leading to an abrupt change of the helix orientation when the energy is minimized at $\Psi=0$ again. In the other words, the orientation of $\mathbf{k}\|\mathbf{H}$ is favorable at $g\mu_B H\leqslant\Delta$ and at $\sqrt{2}\Delta<g\mu_B H$, while the orientation of $\mathbf{k}\perp\mathbf{H}$ is favorable at $\Delta\leqslant g\mu_B H<\sqrt{2}\Delta$. This scenario is exactly observed for $Fe_{1-x}Co_xSi$ in the present study as well as for MnSi in Ref. 16. For example, for $x=0.2$ the integral intensity of the Bragg reflection shows a deep minimum near T_C at $H_{\mathrm{gap}}=40$ mT seen in Fig. 9 and a simultaneous appearance of weak spots with $\mathbf{k}\perp\mathbf{H}$. So we observe the $\mathbf{k}$ flop under applied field from one energetically favorable direction (parallel to the field) to the other (perpendicular to it). This flop gives an indirect experimental evidence for the spin wave gap to be $\Delta\sim g\mu_B H_{\mathrm{gap}}/\sqrt{2}$, which is equal to 0.60, 3.4, and 2.7 μeV for $x=0.5$, 0.2, and 0.15, respectively. As was shown in Ref. 17 the major contribution to the spin wave gap in zero field stems from the interaction between spin waves and is determined by the DM interaction $\Delta_{\mathrm{SW}}^2=d[H_{C2}^2/(4S)]$, where the numerical coefficient $d\sim 1$ cannot be evaluated. Upon decrease of the temperature the anisotropy expressed by the last term in Eq. (1) arises and, thus, changes the energy landscape not allowing the easy $\mathbf{k}$ flop at $H\sim H_{\mathrm{gap}}$ (see, for example, Ref. 24).

C. Magnetic susceptibility

The magnetic susceptibility at low temperatures $T<T^*<T_C$ shows the crossover behavior at $H=H_{C1}$, which is not the case for the relatively high temperatures $T^*<T<T_C$ (see Fig. 2). According to Eq. (1) there are three energy terms determining the orientation of vector $\mathbf{k}$: One related to $H_\parallel$, the second connected to $H_\perp$ and the third one originated from the anisotropy which measure is $g\mu_B H_{C1}$. For the low temperatures we consider two limiting cases: (i) In a very weak magnetic field, when the directions of the helix axes $\mathbf{k}$ are frozen by the local random anisotropy, the $\mathbf{k}$ vectors are randomly oriented. (ii) In a strong field the $\mathbf{k}$ vector is along the field direction and $H_\perp=0$. In the first case for randomly orientated helix axes $H_\perp^2=2H^2/3$, $H_\parallel^2=H^2/3$, and $E_{\mathrm{mag},1}=-g\mu_B SH^2/(3H_{C2})$ where the L term is taken into account as a source of the random anisotropy. For the strong field, when the helix vector is along the field, $H_\perp=0$ and $E_{(\mathrm{mag},2)}=-g\mu_B SH^2/(2H_{C2})$. The magnetic susceptibility is determined as

$$\chi = -\frac{1}{H}\frac{dE_{\mathrm{mag}}}{dH} \tag{11}$$

and one obtains

$$\frac{\chi_1}{\chi_2} = \frac{2}{3} \approx 0.67. \tag{12}$$

This theoretical prediction is in agreement with the experimental data presented in Fig. 2. Indeed, the ratio of the two slopes $\gamma_1/\gamma_2\approx 0.65$. Thus the crossover observed in the magnetization curve at low temperatures is also explained by the presence of the second field-dependent term (quantum term $\sim H_\perp$) in the expression of the magnetic energy [Eq. (1)].

It should be noted that for the relatively high temperatures $T^*<T<T_C$ the anisotropy weakens and is not able to freeze the randomly oriented helix structure. As a result the magnetic susceptibility corresponds to the high-field limit: $\chi=g\mu_B S/H_{C2}$.

VI. CONCLUDING REMARKS

We have carried out polarized neutron diffraction experiments to study the magnetic structure of $Fe_{1-x}Co_xSi$ single crystals with $x=0.10, 0.15, 0.20, 0.50$ in a wide range of temperatures and magnetic fields. It is shown that in zero field $Fe_{1-x}Co_xSi$ has a multidomain left-handed helix structure. For small x the helix axis has a weak tendency to orient along the $\langle 100\rangle$ direction. The magnetic field induces a single domain structure with the helix wave vector oriented along the field axis at $H>H_{C1}$. The field H_{C1} determines the energy of the domain wall in the sample. In the vicinity of T_C the field dependent integral intensity of the Bragg reflection shows a sharp minimum at $H=H_{\mathrm{gap}}$. This phenomenon is well explained by the presence of a spin wave gap $\Delta\sim g\mu_B H_{\mathrm{gap}}/\sqrt{2}$ that provides the stability of the spin wave spectrum with respect to the perpendicular magnetic field. Further increase of the applied field leads to a magnetic phase transition from a conical to a ferromagnetic state close

to H_{C2}. We have evaluated the major interactions of the system (A, Da, and the spin wave gap Δ) from our the experiment using a recently developed theory.[17] We showed that the same set of parameters with different values governs the magnetic system in this compound. In this paper we concentrate on forces defining the orientation of the wave vector in the low field range. As was shown these magnetic properties are ruled by the anisotropy and by two types of the magnetic susceptibility.

The major finding of the study are as follows.

(i) The anisotropy of the system decreases with the increase of the Co concentration x. In our view this is related to a local disorder induced into the system by the substitution of the Fe by Co. The increase of the disorder results in a random distribution of the helix wave vectors $\mathbf{k}$ at large x, whereas $\mathbf{k}$ is oriented along the $\langle 100 \rangle$ axis at small x.

(ii) For all Co concentrations under study the presence of a k flop of the helix wave vector was shown in a narrow field range close to T_C (A phase). This k flop is well explained by the interplay of two competing terms in the magnetic energy: One representing the classical Zeeman energy and the other having a quantum nature [see Eq. (1)].

(iii) The crossover behavior in the magnetization at low temperature is also well explained by the same expression. The agreement between the theory and experiment (Fig. 2) is reached on both the qualitative and quantitative levels.

As a conclusion, we have demonstrated the applicability of the new theory[17] to the $Fe_{1-x}Co_xSi$ compound. The existence of a spin wave gap and a quantum term in the magnetic susceptibility is shown to explain the existing set of the experimental data.

ACKNOWLEDGMENTS

The PNPI team acknowledges GKSS for their hospitality. The work is supported in part by the RFBR (Projects No. 05-02-19889, 06-02-16702, and 07-02-01318) and the Russian State Programs "Quantum Macrophysics" and "Strongly correlated electrons in Semiconductors, Metals, Superconductors and magnetic Materials" and Russian State Program "Neutron research of solids."

[1] C. Pfleiderer, S. R. Julian, and G. G. Lonzarich, Nature (London) **414**, 427 (2001).
[2] C. Pfleiderer, D. Resnik, L. Pintschovius, H. Von Löhneysen, M. Garst, and A. Rosch, Nature (London) **427**, 227 (2004).
[3] P. Bak and M. H. Jensen, J. Phys. C **13**, L881 (1980).
[4] J. Beille, J. Voiron, and M. Roth, Solid State Commun. **47**, 399 (1983).
[5] J. Beille, J. Voiron, F. Towfiq, M. Roth, and Z. Y. Zhang, J. Phys. F: Met. Phys. **11**, 2153 (1981).
[6] K. Ishimoto, H. Yamaguchi, Y. Yamaguchi, J. Suzuki, M. Arai, M. Furusaka, and Y. Endoh, J. Magn. Magn. Mater. **90&91**, 163 (1990).
[7] K. Ishimoto, Y. Yamaguchi, J. Suzuki, M. Arai, M. Furusaka, and Y. Endoh, Physica B **213&214**, 381 (1995).
[8] Y. Ishikawa, K. Tajima, D. Bloch, and M. Roth, Solid State Commun. **19**, 525 (1976).
[9] Y. Ishikawa, G. Shirane, J. A. Tarvin, and M. Kohgi, Phys. Rev. B **16**, 4956 (1977).
[10] B. Lebech, J. Bernhard, and T. Freltoft, J. Phys.: Condens. Matter **1**, 6105 (1989).
[11] I. E. Dzyaloshinskii, Zh. Eksp. Teor. Fiz. **46**, 1420 (1964).
[12] D. Nakamishi, A. Janase, A. Hasejawa, and M. Kitaoka, Solid State Commun. **35**, 995 (1980).
[13] M. Uchida, Y. Onose, Y. Matsui, and Y. Tokura, Science **311**, 359 (2006).
[14] K. Kadowaki, K. Okuda, and M. Date, J. Phys. Soc. Jpn. **51**, 2433 (1982).
[15] Y. Ishikawa and M. Arai, J. Phys. Soc. Jpn. **53**, 2726 (1984).
[16] S. V. Grigoriev, S. V. Maleyev, A. I. Okorokov, Yu. O. Chetverikov, and H. Eckerlebe, Phys. Rev. B **73**, 224440 (2006).
[17] S. V. Maleyev, Phys. Rev. B **73**, 174402 (2006).
[18] M. Bode, M. Heide, K. von Bergmann, P. Ferriani, S. Heinze, G. Bihlmayer, A. Kubetzka, O. Pietzsch, S. Blugel, and R. Wiesendanger, Nature (London) **447**, 05802 (2007).
[19] D. Zur, D. Menzel, I. Jursic, J. Schoenes, L. Patthey, M. Neef, K. Doll, and G. Zwicknagl, Phys. Rev. B **75**, 165103 (2007).
[20] D. Menzel, D. Zur, and J. Schoenes, J. Magn. Magn. Mater. **272-276**, 130 (2004).
[21] N. Manyala, Y. Sidis, J. F. DiTusa, G. Aeppli, D. P. Young, and Z. Fisk, Nature (London) **404**, 581 (2000).
[22] S. V. Maleyev, V. G. Bar'jakhtar, and R. A. Suris, Fiz. Tverd. Tela (S.-Peterburg) **4** 3461 (1962) [Sov. Phys. Solid State **4**, 2533 (1963)].
[23] S. V. Grigoriev, S. V. Maleyev, A. I. Okorokov, Yu. O. Chetverikov, P. Böni, R. Georgii, D. Lamago, H. Eckerlebe, and K. Pranzas, Phys. Rev. B **74**, 214414 (2006).
[24] S. V. Grigoriev, S. V. Maleyev, A. I. Okorokov, Yu. O. Chetverikov, and H. Eckerlebe, J. Phys.: Condens. Matter **19**, 145286 (2007).